Precision Molecular Engineering of Miniaturized Near-Infrared Fluorophores

Rongrong Huang,[+] Qinglong Qiao,[+] Tianruo Shen, Xia Wu, Chao Wang, Nannan Ding, Weijie Chi, Huaming Sun, Zhaochao Xu,* Yu Fang,* Xiaogang Liu*

Dr. R. Huang, T. Shen, Dr. X. Wu, Dr. C. Wang, Prof. Dr. X. Liu
Fluorescence Research Group, Singapore University of Technology and Design, 8 Somapah Road, Singapore 487372 (Singapore). E-mail: xiaogang_liu@sutd.edu.sg

N. Ding, Dr. H. Sun, Prof. Dr. Y. Fang
Key Laboratory of Applied Surface and Colloid Chemistry (Ministry of Education), School of Chemistry and Chemical Engineering, Shaanxi Normal University, Xi'an, Shaanxi 710119 (P. R. China). E-mail: yfang@snnu.edu.cn

Prof. Dr. Q. Qiao, Prof. Dr. Z. Xu
CAS Key Laboratory of Separation Science for Analytical Chemistry, Dalian Institute of Chemical Physics, Chinese Academy of Sciences,457 Zhongshan Road, Dalian 116023 (P. R. China). E-mail: zcxu@dicp.ac.cn

Prof. Dr. W. Chi. Collaborative Innovation Center of One Health, School of Chemistry and Chemical Engineering, Hainan University, Haikou, Hainan 570228 (P. R. China)

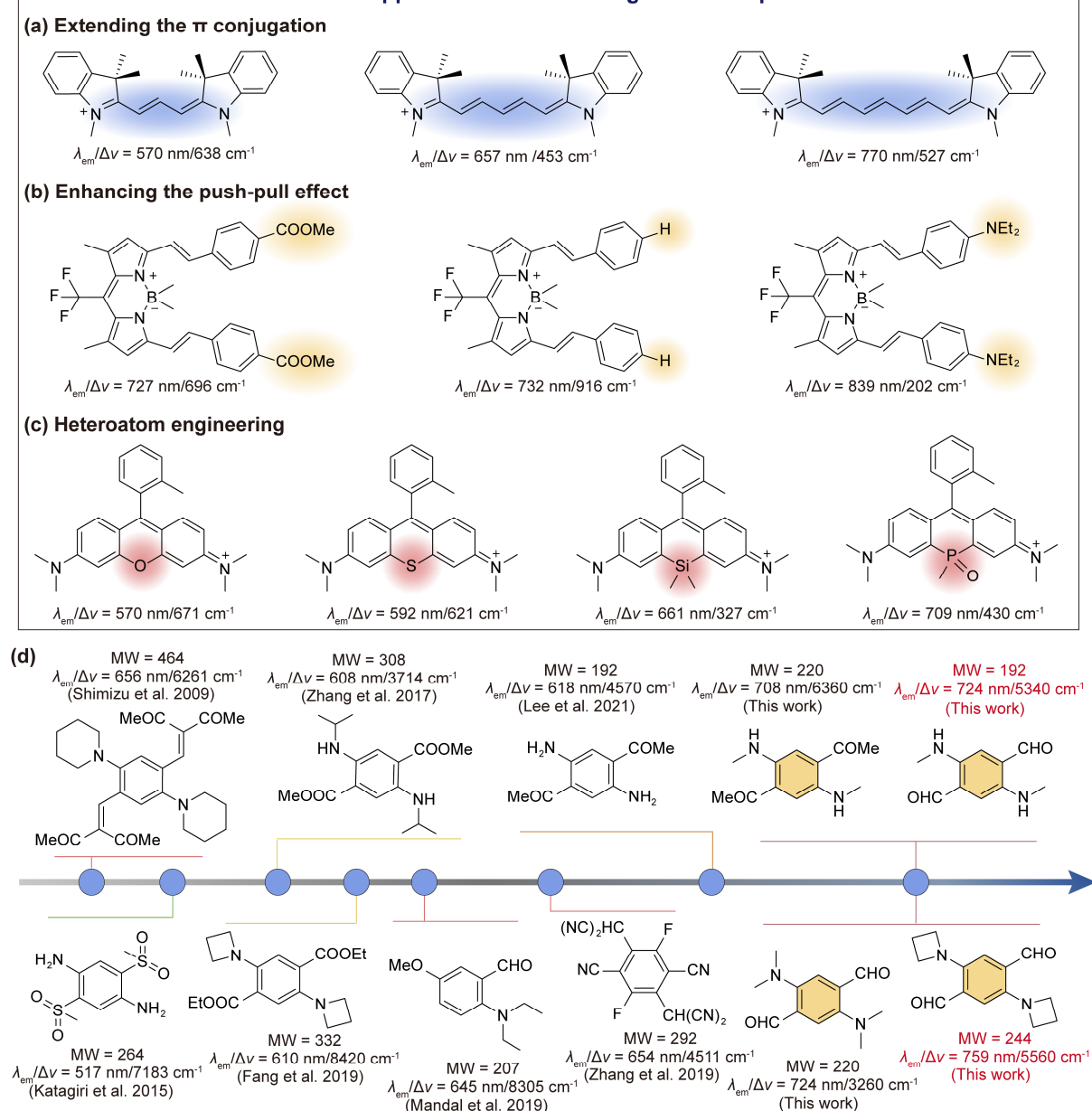[+] These authors contributed equally to this work.

Abstract

Organic fluorophores with near-infrared (NIR) emissions and reduced molecular weights are crucial for advancing bioimaging and biosensing technologies. Traditional methods, such as conjugation expansion and heteroatom engineering, often fail to reduce fluorophore size without sacrificing NIR emission properties. Addressing this challenge, our study utilized computational screening and structure-property relationship analysis to establish comprehensive design principles for compact, single-benzene-based NIR fluorophores. These newly developed fluorophores not only exhibit emissions above 700 nm but also maintain molecular weights under 200 g/mol, approximately 25% of that of Cy7. Additionally, they display unique environmental sensitivity—non-emissive in aqueous solutions but highly emissive in lipid environments. This property significantly enhances their utility in live cell imaging by enabling wash-free applications. Our findings mark a substantial breakthrough in fluorophore engineering, paving the way for more efficient and adaptable imaging methodologies.

1   Introduction

Organic fluorophores have garnered growing interest due to their expansive and promising applications in life sciences and biomedical research (*i.e.*, disease diagnosis, protein quantifications, and the study of cellular/organism dynamics).[1, 2] In these applications, the efficient diffusion of fluorophores and their tight binding to target biomolecules are crucial. To this end, small molecular size is advantageous in improving cell penetrability and minimizing interference with target biomolecules;[3, 4] smaller molecules also contribute to enhanced imaging resolution in advanced super-resolution microscopy.[5] Besides small molecular sizes, the red and near-infrared (NIR) emissions are highly favoured in bioimaging as they enhance penetration depth, reduce auto-fluorescence, and mitigate phototoxicity to cells.[6-9] Consequently, the development of small and red/NIR (SR) fluorophores is in urgent demand but remains a significant challenge.[10]

Scheme 1 *(a-c) Popular strategies to develop red and NIR fluorophores, and the corresponding chemical structures, emission wavelengths (λ; nm) and Stokes shifts (Δν; cm⁻¹) of the representative compounds; (d) Chemical structures, molecular weights (MW), emission wavelengths (λ) and Stokes shifts (Δν) of the selected single-benzene-based fluorophores. The units of MW, λ and Δν are g mol⁻¹, nm, and cm⁻¹, respectively.*

Significant efforts have been made to the development of red and near-infrared (NIR) fluorophores (Scheme 1a-c).[11] One established approach for achieving red or NIR emission involves expanding the π-conjugation of a fluorophore. For example, extending the polymethine chain of cyanine dyes can effectively shift their emission wavelengths into the NIR region.[2, 12, 13] Enhancing intramolecular charge transfer (ICT) provides another alternative route to achieve red/NIR emission.[14] By increasing the donor/acceptor strengths, Suzuki and colleagues developed Keio-BODIPYs with

emissions spanning the visible to NIR region.[15] Heteroatom engineering presents another promising avenue for realizing bathochromic shifts. For instance, replacing the oxygen-bridging atom in the xanthene scaffold with different heteroatoms, such as silicon (Si), sulfur (S), and phosphorus (P), has resulted in a diverse spectrum of colorful rhodamines with emissions covering the visible to NIR range.[16-21] Using the same strategy, Vendrell et al. developed nitrobenzoxadiazole (NBD)-like SCOTfluor emitting in the visible-NIR region.[3] However, many of these classical fluorophores are characterized by substantial molecular sizes, which may disrupt metabolite traffic and impact protein and enzyme function.[22] In fact, red/NIR emissions and small molecular sizes usually contradict each other as a fluorophore with small conjugation typically has a large electronic gap, resulting in short emission wavelengths. Additionally, many of these fluorophores, including rhodamine and cyanine dyes, carry a net charge, which can lead to potential issues such as nonspecific binding to biomolecules.

A unique approach to synthesizing small and red (SR) fluorophores involves attaching single or multiple donors and acceptors to a single phenyl ring,[23-26] as depicted in Scheme 1d. Shimizu and colleagues made a significant contribution to this field by developing a series of single benzene-based fluorophores,[27] achieving peak emission wavelengths (λ_{em}) up to 656 nm (in cyclohexane; molecular weight (MW) = 465 g/mol). Katagiri and team later synthesized the first benzene-based fluorophore with a molecular weight under 300 g/mol,[28] while preserving green fluorescence (λ_{em} = 517 nm in water). This field was further advanced by Mandal,[29] Fang[30] and Zhang[31, 32] et al., who extended the emission wavelengths of single-benzene based fluorophores to >600 nm, while maintaining molecular weights below 350 g/mol. Additionally, Lee et al. serendipitously developed a red fluorophore *p*-DAPA,[33] characterized by its minimal size (λ_{em} = 618 nm; MW = 192 g/mol). However, the emission wavelengths of these compact fluorophores are predominantly confined to the visible spectrum (< 700 nm), and their practical applications have yet to be fully explored. More critically, precise molecular design principles to steer the systematic engineering of SR fluorophores remain undeveloped.

In this study, we leveraged quantum chemical calculations and molecular screening, coupled with an in-depth structure-property relationship analysis, to

rationally design near-infrared (NIR) dyes of exceptionally small size (λ_{em} of up to 759 nm in ethanol; MW of down to 192 g/mol). We systematically identified various factors influencing the spectral properties of these dyes, including substituent positional effects, push-pull dynamics, and the impact of steric hindrance, illuminating pathways for further molecular engineering of small and red fluorophores. Notably, the fluorophores developed through this method exhibit outstanding environmental sensitivities and fluorogenicity, facilitating wash-free super-resolution imaging of lipid droplets in live cells.

2　Results and Discussion

2.1　Molecular Screening of Single Benzene-Based Fluorophores

To establish comprehensive guidelines for designing single benzene-based small and red (SR) fluorophores, our study commenced with the computational modeling of representative single-benzene derivatives. Our objective is to assess the effects of substituent positions, as well as the influence of differing numbers of donors and acceptors, on the peak UV-vis absorption (λ_{abs}) and emission wavelengths (λ_{em}). In these models, $-NH_2$ (amine) and -CN (cyano) were selected as the donor (D) and acceptor (A) groups, respectively, due to their small sizes which help minimize steric repulsion and potential non-emissive bending of the fluorophore scaffold. We explored various donor-acceptor ratios in three series: 1:1 (A series, Figure 1a), 2:2 (B series, Figure 1b), and 3:3 (C series, Figure 1c), attaching these groups at different positions on the benzene scaffold. Our results indicated that compounds A2, B9, and C2 exhibit the longest emission wavelengths in their respective series, with calculated λ_{em} at 338, 496, and 499 nm (Figure 1d), respectively.

The 1D-1A system (A series) showed less satisfactory emission wavelengths due to small molecular sizes and limited π-conjugation. The 3D-3A system (C2) demonstrated slightly longer emission wavelengths; however, substantial scaffold distortion occurred with larger D/A fragments (*e.g.*, azetidine and -CHO), leading to non-emissive states in such heavily substituted benzene scaffolds (Figure S6). Thus, the 2D-2A system (B9) emerged as an ideal candidate for further in silico molecular engineering.

Further investigation into the frontier molecular orbitals elucidated the molecular origin of the favourable D/A arrangement in B9 for extended $\lambda_{abs}/\lambda_{em}$. For example, in
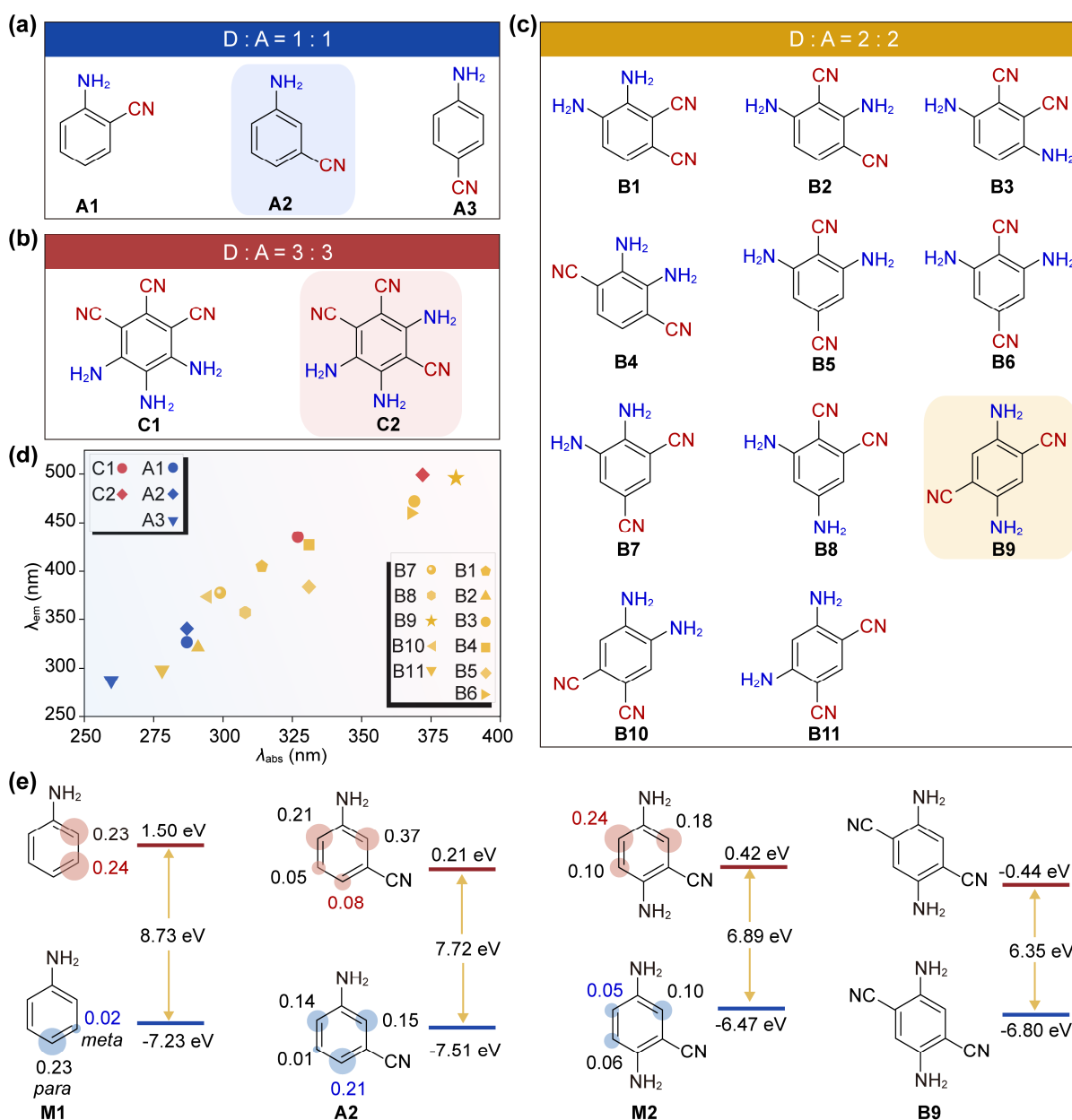
Fig. 1 (a-c) Chemical structures of SR fluorophores with the ratio of the number of donor and acceptor fragments fixed at 1:1, 2:2, and 3:3; (d) The calculated peak UV-vis absorption and emission wavelengths. All calculations are performed at the ωB97XD/Def2SVP level in DMSO; (e) The atomic contributions to HOMO and LUMO of single benzene-based molecules, and the calculated HOMO/LUMO energy levels and corresponding electronic gaps. The calculations are based on the optimized S_1 structures in DMSO. Blue: atomic contributions to HOMO; Red: atomic contributions to LUMO. The numbers in color highlight the substitution positions with significant changes in atomic contributions.

the *meta*-position of the 1D-substituted compound M1 (Figure 1e), we observed minimal electron density in the highest occupied molecular orbital (HOMO) and a high density in the lowest unoccupied molecular orbital (LUMO). Placing an acceptor at this *meta*-position to the donor in M1 would significantly stabilize/lower the LUMO with minimal impact on the HOMO, reducing the electronic gap and leading to large bathochromic shifts. This was exemplified in the 1D-1A compound A2, where the

acceptor is at the *meta*-position to the donor, yielding the longest λ_{em} in the A Series (1D-1A). Similarly, in M1 and A2, notable electron density at the *para*-position in the HOMO, which significantly reduces in the LUMO, suggested that adding a donor at the *para*-position would raise/destabilize the HOMO while minimally affecting the LUMO, facilitating red shifts.[34, 35] This red shift is evidenced by the significant change from A2 to M2. The most effective red shift was achieved by combining two pairs of donors and acceptors: two D fragments are positioned *para* to each other (as were the acceptors). Additionally, each A fragment is positioned *meta* to a D fragment. This substitution pattern exactly matches that of B9.

2.2 In Silico Molecular Engineering of the Single Benzene-Based NIR Fluorophores

Guided by the substitution pattern observed in B9, our subsequent investigations focused on the impact of varying the electron-donating and -accepting strength of the D/A fragments on the λ_{abs} and λ_{em} of benzene-based SR fluorophores (Figure 2). By retaining -CN (exhibiting minimal steric hindrance) as the acceptor, an increase in the electron-donating strength of the donor from -OH to azetidine resulted in a red shift of calculated λ_{em} from 370 to 541 nm (Figures 2a, 2c). Similarly, maintaining -NH_2 (also with small steric hindrance) as the donor, a progressive increase in the electron-withdrawing strength of the acceptor from -F to -CHO led to a bathochromic shift from 367 to 609 nm (Figures 2b, 2c). These findings underscore that enhanced charge transfer can significantly amplify the bathochromic shifts.

Steric hindrance also plays a pivotal role in influencing the red shifts of λ_{abs} and λ_{em} by impacting the planarity (and the conjugation) of the fluorophore. When opting for the aldehyde group (which poses a large steric hindrance) as the acceptor (F series, Figure 2d), the methylamine donor (F1) induces the most significantly red-shifted emission. However, stronger donors like dimethylamine (F2) and azetidine (F3) result in blue shifts in comparison to F1. A detailed analysis of the optimized ground state geometries reveals that the D fragments in F2 and F3 exhibit pre-twisted or bent structures due to strong steric repulsion with the aldehyde acceptor. This non-planarity hinders effective charge delocalization, contributing to the blue shift in F2 and F3 compared to F1 (Figure 2d). In contrast, the methylamine-substituted F1, due to lesser steric hindrance and the formation of an intramolecular

hydrogen bond, maintains excellent planarity, emerging as a promising candidate for small and red fluorophores.
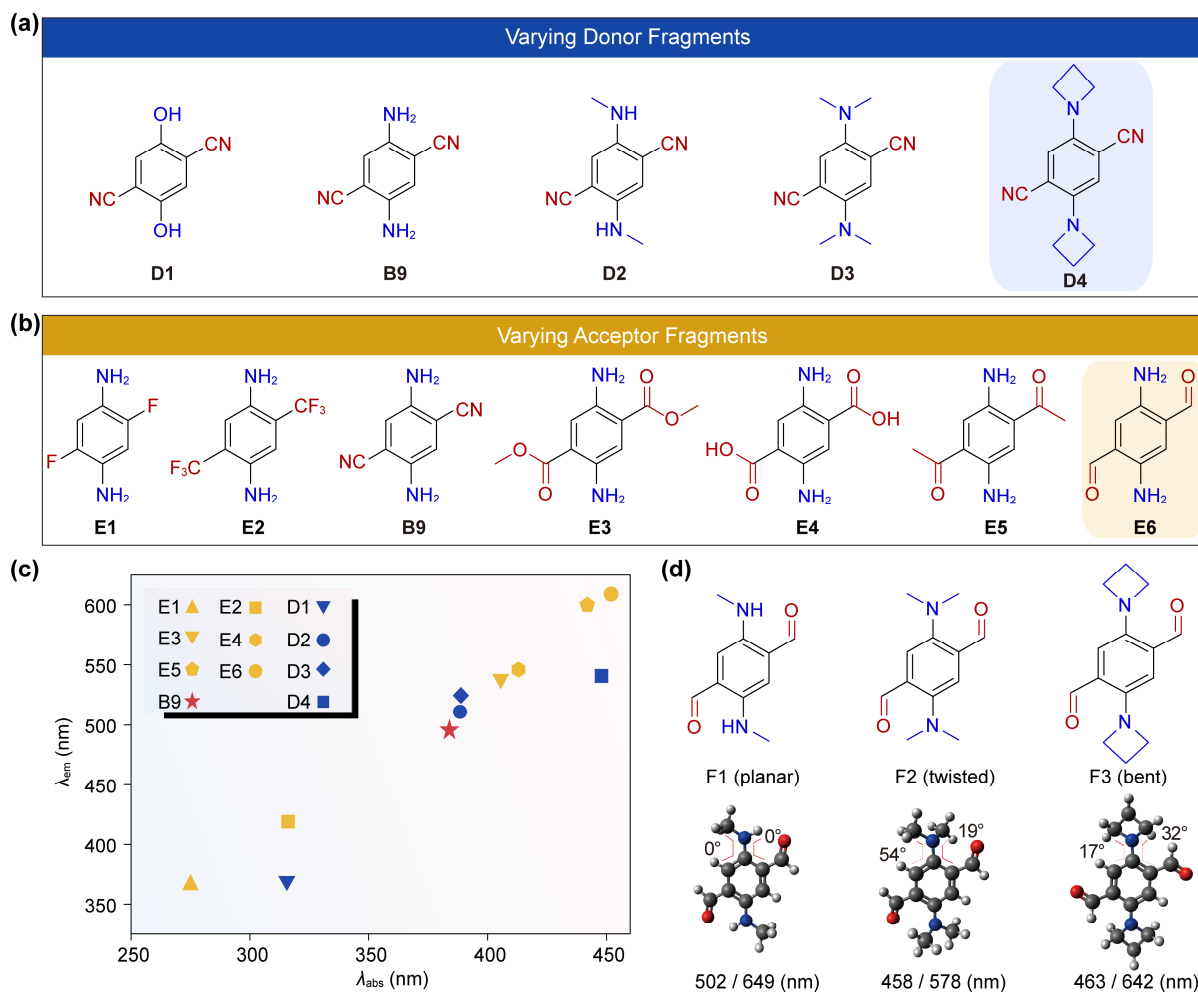

Fig. 2 (a, b) Chemical structures of single benzene-based fluorophores with different donor and acceptor fragments. (c) Calculated UV-vis absorption and emission wavelengths of different fluorophores including B9, D series, and E series. (d) Chemical structures of F series with different donors and a -CHO acceptor, their optimized ground-state (S_0) structures, as well as the calculated UV-vis absorption and emission wavelengths. Note: the calculations were performed at the ωB97XD/Def2SVP level in DMSO.

This thorough structure-property relationship study of single-benzene fluorophores inspired the design of a series of SR fluorophores with two D-A pairs. Notably, SR-1, SR-3, SR-5, and SR-7 exhibit longer calculated emission wavelengths than popular NIR fluorophores like Cy5 and Si-Rhodamine (Figure S10). It is important to acknowledge the systematic drift inherent in quantum chemical calculations. However, the relative differences between these compounds suggest that emissions of several single-benzene fluorophores reach the NIR region. The sizes of the SR fluorophores, in terms of molecular weight, are significantly smaller

(by approximately 50%) than those of Cy5 and Si-Rhodamine. Among these, SR-1 or SR-3 are potential candidates for the smallest NIR dyes reported to date.

2.3 Chemical Synthesis, Structure, and Spectral Characterization

Building on the insights from our theoretical analysis, 11 single-benzene fluorophores were designed and synthesized (Figure 3). In agreement with theoretical modeling, the crystallography data revealed that the methylamino-substituted SR-5 maintains excellent planarity, forming an intramolecular hydrogen bond between the methylamino and acetyl groups. In contrast, significant pretwisting was observed in the dimethylamino group of SR-2 and SR-6, with the dihedral angles reaching approximately 69° and 59° for SR-2 and SR-6, respectively (Figure S11). These findings underscore the importance of managing steric hindrance to preserve the planarity of fluorophores, especially as the number of D/A substituents increases.

Subsequent spectral measurements of these compounds in solvents of varying polarity (Figures 3b, S15-17) revealed that SR-1, SR-2, SR-3, and SR-5 exhibit NIR emissions, peaking at 724, 724, 759, and 708 nm in ethanol (Figure 3c), respectively. We compared the λ_{em} of these single-benzene fluorophores and their molecular weights (Figure S18), with those of popular NIR fluorophores and previously reported single benzene-based fluorophores (Figure S19). Our analysis suggests that SR-1 is likely the smallest NIR dye reported to date.

These experimental spectral data align well with our theoretical predictions. For instance, enhancing the donor strength from -NH$_2$ to -NHCH$_3$ led to an increased red shift, with λ_{em} recorded at 676 (SR-4) and 708 (SR-5) nm in ethanol (Figure 3c), respectively. Similarly, strengthening the acceptor from -COOCH$_3$ to -COCH$_3$ and -CHO resulted in a noticeable red shift from 592 (SR-11) to 681 (SR-7) and 759 (SR-3) nm in ethanol (Figure 3c). Notably, the planar SR-1, SR-4, and SR-5 exhibited longer λ_{abs} and λ_{em} wavelengths than the pretwisted SR-3 and SR-6 (Table S1, Figure 3c) in their corresponding solvents, which aligns with the quantum chemical calculations.

A significant solvatochromic effect was observed in these compounds (Figures S15-17, Table S1) due to intense intramolecular charge transfer. For example, the λ_{em} of SR-3 shifted from 631 nm in n-hexane to 759 nm in ethanol (Figure 3b),

illustrating the impact of the solvent environment on the spectral properties of these fluorophores.
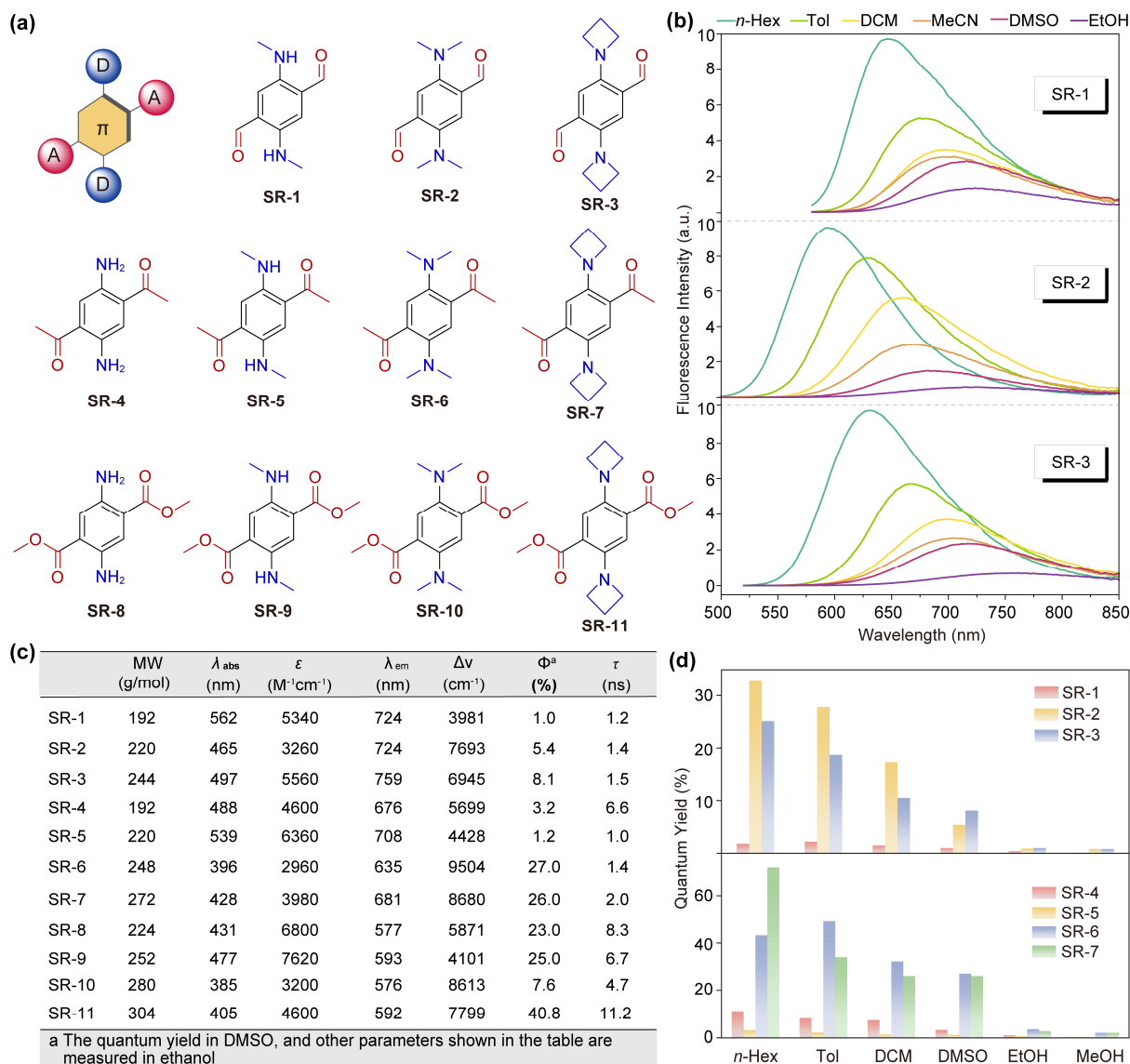

Fig. 3 (a) Chemical structures of SR fluorophores. (b) Emission spectra of SR-1, SR-2 and SR-3 in different solvents. (c) The photophysical properties of SR fluorophores. (d) Fluorescence quantum yields of SR-1, SR-2, SR-3, SR-4, SR-5, SR-6 and SR-7 in different solvents. The concentrations of the samples are 50 µM.

(c)

	MW (g/mol)	λ_{abs} (nm)	ε ($M^{-1}cm^{-1}$)	λ_{em} (nm)	$\Delta\nu$ (cm^{-1})	Φ^a (%)	τ (ns)
SR-1	192	562	5340	724	3981	1.0	1.2
SR-2	220	465	3260	724	7693	5.4	1.4
SR-3	244	497	5560	759	6945	8.1	1.5
SR-4	192	488	4600	676	5699	3.2	6.6
SR-5	220	539	6360	708	4428	1.2	1.0
SR-6	248	396	2960	635	9504	27.0	1.4
SR-7	272	428	3980	681	8680	26.0	2.0
SR-8	224	431	6800	577	5871	23.0	8.3
SR-9	252	477	7620	593	4101	25.0	6.7
SR-10	280	385	3200	576	8613	7.6	4.7
SR-11	304	405	4600	592	7799	40.8	11.2

a The quantum yield in DMSO, and other parameters shown in the table are measured in ethanol

2.4 Molecular Origins of the Environmental Sensitivity

We observed not only favorable red/NIR emissions, but also significant environmental sensitivity in the quantum yields of the single benzene fluorophores (*i.e.*, SR-1, SR-2, SR-3, SR-4, SR-5, SR-6, SR-7). This environmental sensitivity is attributable to several mechanisms, including hydrogen bond-induced quenching and twisted intramolecular charge transfer (TICT).[36, 37]

Hydrogen bonding interactions with solvent molecules profoundly influence the fluorescence of these single-benzene fluorophores. For instance, SR-3 exhibits moderate fluorescence in aprotic solvents (quantum yield φ = 8% in DMSO) but becomes non-emissive in protic solvents (φ ≈ 0 in ethanol and methanol, Figure 3d). To predict the fluorophore's quantum yield susceptibility to hydrogen bond-induced quenching in protic solvents, we have developed a descriptor, Δ.[38] Δ quantifies the absolute changes in charge density during the HOMO-LUMO transition at the hydrogen bond donating site of the fluorophore. A large Δ value indicates significant perturbation to the hydrogen bond equilibrium in the ground state during photoexcitation, leading to substantial vibrations between the dye and surrounding solvents during the re-establishment of the hydrogen bond equilibrium in the excited state. Hence, a large Δ suggests substantial vulnerability of quantum yields to hydrogen bond-induced quenching, resulting in lower quantum yields in protic solvents. Our findings show that most of these fluorophores (except of SR-10 and SR-11) display large Δ values (ranging from 0.17 to 0.21), indicating generally lower quantum yields in protic than in aprotic solvents.

Intramolecular hydrogen bonds also contribute to lower quantum yields, as evidenced by comparing analog compounds SR-1 and SR-3, as well as SR-5 and SR-7 (Figure S25). SR-1, with an intramolecular hydrogen bond, exhibits significantly lower quantum yields than SR-3 which lacks such a bond, across all solvents. We studied the geometrical changes of SR-1 upon photoexcitation in n-hexane. our calculations reveal a significant strengthening of the intramolecular hydrogen bond in SR-1, evidenced by a reduction in the O···H distance from 1.94 Å to 1.78 Å (Figures S26a, b). We also analysed the Huang-Rhys factors and reorganization energy contributions as a function of vibrational modes in SR-1. The major Huang-Rhys factor and significant reorganization energy contribution in the low-frequency region (λ < 250 cm-1) are related to vibrations along the intramolecular hydrogen bond (Figures S26c, d). The intramolecular charge transfer from the donor to the acceptor alters the charge density around the amino and oxygen atoms, causing the hydrogen atom in the bond to move closer to the oxygen atom. This considerable movement accelerates non-radiative decay, thereby lowering quantum yields.

Significant TICT formation was observed in these single-benzene derivatives. For example, the pre-twisted SR-2 displays a lower energy barrier and a strong

driving force towards TICT (Figure 4b), wherein the -N(CH$_3$)$_2$ rotates to become perpendicular to the fluorophore scaffold, resulting in complete charge separation and a zero oscillator strength (*f*) (Figure S32). Similar TICT formations were observed in SR-3, SR-6, SR-7, SR-10 and SR-11 (Figure S31). By substituting the dimethylamino group with an azetidine group, the TICT tendency was notably reduced, reflected in higher energy barriers and lower driving energy.[39, 40] Consequently, the quantum yield (*φ*) of SR-3 is generally higher than that of SR-2.

We also explored the possibility of excited-state intramolecular proton transfer (ESIPT) in fluorophores with an intramolecular hydrogen bond. However, our calculations do not support the energetic feasibility of ESIPT (Figure S27).

2.5 Transient Absorption Studies

To validate our computational findings on the fluorescence quenching channels, we further collected transient absorption (TA) spectra of SR-1 and SR-2 in three distinct solvents (*n*-hexane, DMSO, and ethanol).

TA spectra corroborate hydrogen bond-induced quenching in SR-1 (Figures 4d, 4e). In non-protic solvents, such as *n*-hexane (Figure 4d) and DMSO (Figure S33b), we did not observe significant peak shifts in the TA spectra of SR-1. The excited state has a long lifetime, and notable decay starts to appear after >100 picoseconds. In contrast, the TA spectra of SR-1 in ethanol (polar and protic solvent) exhibit two excited state absorption (ESA) bands that mainly peaked at ~650 and ~660 nm, respectively. About 45 ps after the photoexcitation, the first band starts to decay, and the second band emerges, along with the formation of an isosbestic point at ~703 nm (Figure S33b). This new band exhibits a decay time of ~1.0 ns, which is very close to the fluorescent lifetime (Table S1). We inferred that the intermolecular hydrogen bonding interactions between SR-1 and surrounding ethanol molecules may induce further stabilization of the ICT state to yield a relaxed ICT state (Figures 4e, S34c), leading to the slight shift of the TA spectral peaks. In this relaxed state, the stimulated emission (SE) band becomes very weak, indicating that the hydrogen
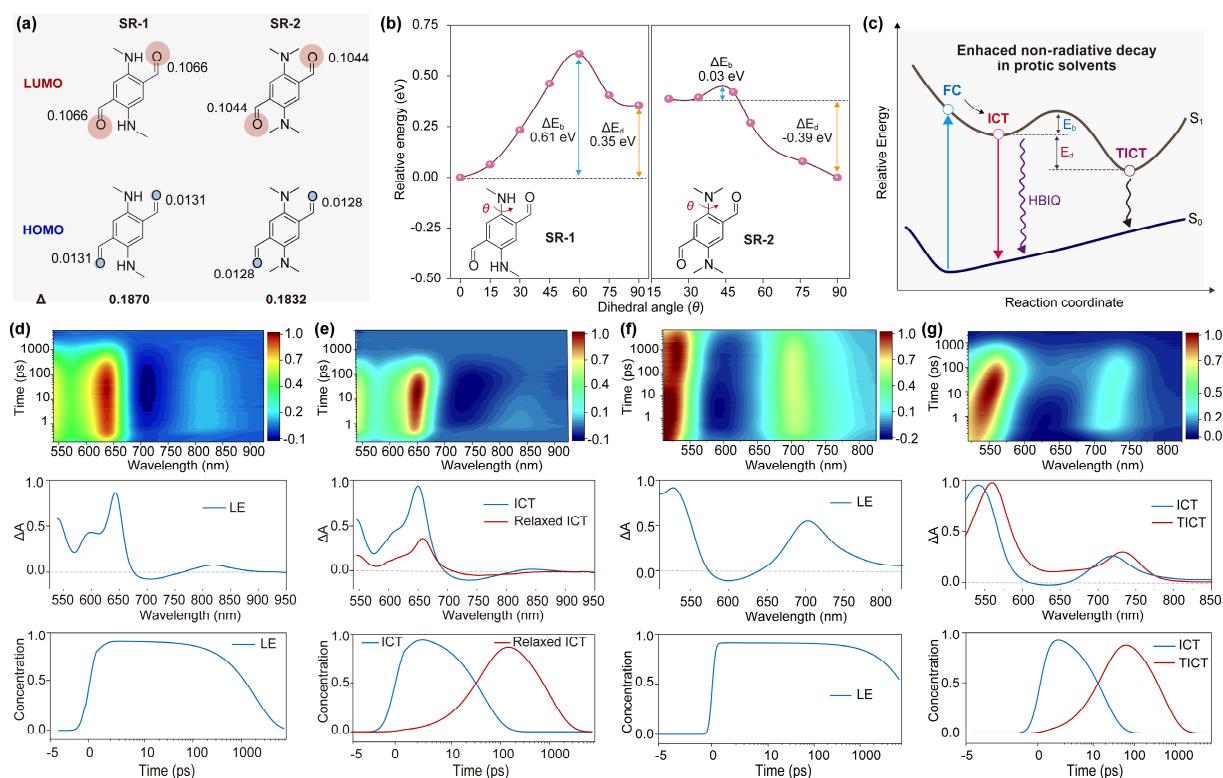
Fig. 4 (a) Atomic contributions to the HOMO and LUMO of SR-1 and SR-2 calculated based on the optimized S_0 structure in DMSO. Blue: atomic contribution to HOMO; red: atomic contribution to LUMO. Δ represents the sum of the absolute change of atomic contributions of HOMO and LUMO at each hydrogen bond accepting site (highlighted in blue and red). (b) The relative electronic energy of the S_1 potential energy surfaces of SR-1 (left) and SR-2 (right) as a function of dihedral angle θ. Insets show the chemical structures, the dihedral angle (θ), the energy barrier (ΔE$_b$) and driving energy (ΔE$_d$) to enter their corresponding TICT states. All calculations were performed at the ωB97XD/Def2SVP level of theory in DMSO. (c) Proposed mechanism scheme of the SR fluorophores illustrating the energy barrier to enter the TICT state, as well as the radiative and non-radiative decay pathway in polar protic solvents; major fluorescence quenching channels include hydrogen bond induced quenching (HBIQ) and TICT. (d, e) Transition absorption data of SR-1 pumped at 535 nm in n-hexane (d) and ethanol (e). (f, g) Transition absorption data of SR-2 pumped at 450 nm in n-hexane (f) and ethanol (g). The top panel: TA contour; the middle panel: species-associated spectra plots; the bottom panel: relative population profiles of the excited state species.

bond interactions induced vibrations greatly quench the fluorescence. Similar phenomena were observed in SR-5, which also demonstrates hydrogen bonding sensitivity (Figures S39, S40). Finally, our analysis shows that SR-1 is not susceptible to TICT, while the TICT-active SR-2 exhibits distinct TA spectral features.

In *n*-hexane (apolar solvent, Figure 4f), SR-2 exhibits the locally excited (LE) emission which is transformed from the Franck-Condon (FC) state via minor structural relaxation. Within the early time window (< 25 ps), the intensity of the ESA peak (~530 nm) shows little shifts, and the ESA peak at ~710 nm increases along with the narrowing of the edge at 725-800 nm. This phenomenon may be caused by the "cooling" of different vibration states in the excited state. The process from the

FC state to the LE state is ultrafast, which is beyond the detection limit of our system.[14, 41] However, the isosbestic points at ~670 and ~565 nm indicate the presence and deactivation of the LE state. The fitted decay time of the LE state is ~15 ns, which is consistent with the fluorescence lifetime. In ethanol (Figure 4g), SR-2 displays two distinct ESA bands at ~560 and 730 nm, accompanied by a minimal SE signal. This observation aligns with the trend of SR-2 exhibiting low fluorescence quantum yield in polar solvents. Moreover, the two ESA peaks in ethanol exhibit noticeable shifts as time extends, strongly indicating the formation of a new excited state (*i.e.*, from the ICT state to the TICT state, Figures 4c, S36c). The population profiles also indicate that the decrease in the ICT species is accompanied by the increase of the TICT population. Further fitting analysis of the TA spectra suggests the transformation rate from the ICT state to the TICT state is about 18 ps^{-1}. The ICT state decays to the ground state with a time constant of ~1.4 ns, while the non-emissive TICT state decays to the ground state with a time constant of ~500 ps. Similar patterns were also observed in compounds SR-3 (Figures S37, S38), SR-6 (Figures S41, S42) and SR-7 (Figures S43, S44), further substantiating our computational predictions of the TICT quenching channels.

3 Conclusion

In this study, we have successfully established detailed molecular design guidelines for the development of near-infrared (NIR) fluorophores characterized by their notably compact structure. This was achieved through the strategic attachment of two electron-donating and two electron-accepting groups to a single benzene ring. Our approach emphasized the critical role of the positioning of these substituents, the augmentation of push-pull electronic effects, and the meticulous control of steric hindrance. These concerted design strategies yielded fluorophores with an emission spectrum that effectively extends into the NIR region with minimal molecule weight (< 200 g/mol). Notably, these fluorophores demonstrated remarkable environmental sensitivity, exhibiting intense luminescence in aprotic solvents while undergoing pronounced quenching in aqueous environments. This unique property was leveraged to achieve wash-free bioimaging of lipid droplets in live cells. The design methodology of this research not only provides a blueprint for the molecular engineering of compact NIR fluorophores but also opens avenues for exploring their applications in diverse scientific and technological domains.

Conflicts of Interest

The authors have filed a patent to protect the novel molecular structures of small and red/near-infrared dyes, identified under Singapore Patent Application No. 10202303371R, titled "Singapore Red: Red/Near-Infrared Dyes with Minimal Sizes."

Acknowledgements

4 Reference

1. Grimm, J. B.; Lavis, L. D., Caveat Fluorophore: An Insiders' Guide to Small-Molecule Fluorescent Labels. *Nat. Methods* **2022,** *19* (2), 149-158.

2. Zeng, S.; Liu, X.; Kafuti, Y. S.; Kim, H.; Wang, J.; Peng, X.; Li, H.; Yoon, J., Fluorescent Dyes Based on Rhodamine Derivatives for Bioimaging and Therapeutics: Recent Progress, Challenges, and Prospects. *Chem. Soc. Rev.* **2023,** *52* (16), 5607-5651.

3. Benson, S.; Fernandez, A.; Barth, N. D.; de Moliner, F.; Horrocks, M. H.; Herrington, C. S.; Abad, J. L.; Delgado, A.; Kelly, L.; Chang, Z.; Feng, Y.; Nishiura, M.; Hori, Y.; Kikuchi, K.; Vendrell, M., SCOTfluors: Small, Conjugatable, Orthogonal, and Tunable Fluorophores for In Vivo Imaging of Cell Metabolism. *Angew. Chem. Int. Ed.* **2019,** *58* (21), 6911-6915.

4. Benson, S.; de Moliner, F.; Tipping, W.; Vendrell, M., Miniaturized Chemical Tags for Optical Imaging. *Angew. Chem. Int. Ed.* **2022,** *61* (34), e202204788.

5. Balzarotti, F.; Eilers, Y.; Gwosch, K. C.; Arvid H. Gynnå; Westphal, V.; Stefani, F. D.; Elf, J.; Hell, S. W., Nanometer Resolution Imaging and Tracking of Fluorescent Molecules with Minimal Photon Fluxes. *Science* **2017,** (355), 606-612.

6. Vahrmeijer, A. L.; Hutteman, M.; van der Vorst, J. R.; van de Velde, C. J. H.; Frangioni, J. V., Image-Guided Cancer Surgery Using Near-Infrared Fluorescence. *Nat. Rev. Clin. Oncol.* **2013,** *10* (9), 507-518.

7. Weissleder, R., A Clearer Vision for In Vivo Imaging. *Nat. Biotechnol.* **2001,** *19* (4), 316-316.

8. Guo, Z.; Park, S.; Yoon, J.; Shin, I., Recent Progress in the Development of Near-Infrared Fluorescent Probes for Bioimaging Applications. *Chem. Soc. Rev.* **2014,** *43* (1), 16-29.

9. Yan, K.; Hu, Z.; Yu, P.; He, Z.; Chen, Y.; Chen, J.; Sun, H.; Wang, S.; Zhang, F., Ultra-Photostable Small-Molecule Dyes Facilitate Near-Infrared Biophotonics. *Nat. Commun.* **2024,** *15* (1), 2593.

10. Seah, D.; Cheng, Z.; Vendrell, M., Fluorescent Probes for Imaging in Humans: Where Are We Now? *ACS Nano* **2023,** *17* (20), 19478-19490.

11. Dai, M.; Yang, Y. J.; Sarkar, S.; Ahn, K. H., Strategies to Convert Organic Fluorophores into Red/Near-Infrared Emitting Analogues and Their Utilization in Bioimaging Probes. *Chem. Soc. Rev.* **2023,** *52* (18), 6344-6358.

12. Mishra, A.; Behera, R. K.; Behera, P. K.; Mishra, B. K.; Behera, G. B., Cyanines During the 1990s: A Review. *Chem. Rev.* **2000,** *100* (6), 1973-2012.

13. Zhang, F.; Tang, B. Z., Near-Infrared Luminescent Probes for Bioimaging and Biosensing. *Chem. Sci.* **2021,** *12* (10), 3377-3378.

14. Yu, L.; Abbas Abedi, S. A.; Lee, J.; Xu, Y.; Son, S.; Chi, W.; Li, M.; Liu, X.; Park, J. H.; Kim, J. S., Blending Low‐Frequency Vibrations and Push–Pull Effects Affords Superior Photoacoustic Imaging Agents. *Angew. Chem. Int. Ed.* **2023,** *62* (32).

15. Umezawa, K.; Nakamura, Y.; Makino, H.; Citterio, D.; Suzuki, K., Bright, Color-Tunable Fluorescent Dyes in the Visible-Near-Infrared Region. *J. Am. Chem. Soc.* **2008,** *130* (5), 1550-1551.

16. Zhou, W.; Fang, X.; Qiao, Q.; Jiang, W.; Zhang, Y.; Xu, Z., Quantitative Assessment of Rhodamine Spectra. *Chin. Chem. Lett.* **2021,** *32* (2), 943-946.

17. Chi, W.; Qi, Q.; Lee, R.; Xu, Z.; Liu, X., A Unified Push–Pull Model for Understanding the Ring-Opening Mechanism of Rhodamine Dyes. *J. Phys. Chem. C* **2020,** *124* (6), 3793-3801.

18. Koide, Y.; Urano, Y.; Hanaoka, K.; Terai, T.; Nagano, T., Development of an Si-Rhodamine-Based Far-Red to Near-Infrared Fluorescence Probe Selective for Hypochlorous Acid and Its Applications for Biological Imaging. *J. Am. Chem. Soc.* **2011,** *133* (15), 5680-5682.

19. Fu, M.; Xiao, Y.; Qian, X.; Zhao, D.; Xu, Y., A Design Concept of Long-Wavelength Fluorescent Analogs of Rhodamine Dyes: Replacement of Oxygen with Silicon Atom. *Chem. Commun.* **2008,** *15* (15), 1780-1782.

20. Liu, J.; Sun, Y.-Q.; Zhang, H.; Shi, H.; Shi, Y.; Guo, W., Sulfone-Rhodamines: A New Class of Near-Infrared Fluorescent Dyes for Bioimaging. *ACS Appl. Mater. Interfaces* **2016,** *8* (35), 22953-22962.

21. Chi, W.; Tan, D.; Qiao, Q.; Xu, Z.; Liu, X., Spontaneously Blinking Rhodamine Dyes for Single-Molecule Localization Microscopy. *Angew. Chem. Int. Ed.* **2023,** *62* (39), e202306061.

22. Jin, J. H.; An, J. M.; Kim, D.; Lee, S.; Kim, M.; Kim, D., Amino-SBBF (Single Benzene-based Fluorophore) Library: Its Synthesis, Photophysical Property, and Cellular Imaging Application. *Dyes and Pigm.* **2024,** *221*.

23. Zhang, J. N.; Kang, H.; Li, N.; Zhou, S. M.; Sun, H. M.; Yin, S. W.; Zhao, N.; Tang, B. Z., Organic Solid Fluorophores Regulated by Subtle Structure Modification: Color-Tunable and Aggregation-Induced Emission. *Chem. Sci.* **2017,** *8* (1), 577-582.

24. Kim, H.; Kim, Y.; Lee, D., Small is Beautiful: Electronic Origin and Synthetic Evolution of Single-Benzene Fluorophores. *Acc. Chem. Res.* **2023,** *57* (1), 140-152.

25. Tang, B.; Wang, C.; Wang, Y.; Zhang, H., Efficient Red-Emissive Organic Crystals with Amplified Spontaneous Emissions Based on a Single Benzene Framework. *Angew. Chem. Int. Ed.* **2017,** *56* (41), 12543-12547.

26. Chatterjee, T.; Mandal, M.; Mardanya, S.; Singh, M.; Saha, A.; Ghosh, S.; Mandal, P. K., *meta*-Fluorophores: An Uncharted Ocean of Opportunities. *Chem. Commun.* **2023,** *59* (97), 14370-14386.

27. Shimizu, M.; Takeda, Y.; Higashi, M.; Hiyama, T., 1,4-Bis(alkenyl)-2,5-Dipiperidinobenzenes: Minimal Fluorophores Exhibiting Highly Efficient Emission in the Solid State. *Angew. Chem. Int. Ed.* **2009,** *48* (20), 3653-6.

28. Beppu, T.; Tomiguchi, K.; Masuhara, A.; Pu, Y. J.; Katagiri, H., Single Benzene Green Fluorophore: Solid-State Emissive, Water-Soluble, and Solvent- and pH-Independent Fluorescence with Large Stokes Shifts. *Angew. Chem. Int. Ed.* **2015,** *54* (25), 7332-5.

29. Mandal, M.; Chatterjee, T.; Das, A.; Mandal, S.; Sen, A.; Ta, M.; Mandal, P. K., *meta*-Fluors—A Unique Way to Create a 200 Da Ultrasmall Fluorophore Emitting in Red with Intense Stokes/Solvatochromic Shift: Imaging Subcellular Nanopolarity in Live Stem Cells. *J. Phys. Chem. C* **2019,** *123* (40), 24786-24792.

30. Liu, H.; Yan, S.; Huang, R.; Gao, Z.; Wang, G.; Ding, L.; Fang, Y., Single-Benzene-Based Solvatochromic Chromophores: Color-Tunable and Bright Fluorescence in the Solid and Solution States. *Chem. Eur. J.* **2019,** *25* (72), 16732-16739.

31. Xiang, Z.; Wang, Z. Y.; Ren, T. B.; Xu, W.; Liu, Y. P.; Zhang, X. X.; Wu, P.; Yuan, L.; Zhang, X. B., A General Strategy for Development of a Single Benzene Fluorophore with Full-Color-Tunable, Environmentally Insensitive, and Two-Photon Solid-State Emission. *Chem. Commun.* **2019,** *55* (76), 11462-11465.

32. Tang, B.; Wang, C.; Wang, Y.; Zhang, H., Efficient Red‑Emissive Organic Crystals with Amplified Spontaneous Emissions Based on a Single Benzene Framework. *Angew. Chem. Int. Ed.* **2017,** *56* (41), 12543-12547.

33. Kim, H.; Park, W.; Kim, Y.; Filatov, M.; Choi, C. H.; Lee, D., Relief of Excited-State Antiaromaticity Enables the Smallest Red Emitter. *Nat. Commun.* **2021,** *12* (1), 5409.

34. Liu, X.; Cole, J. M.; Xu, Z., Substantial Intramolecular Charge Transfer Induces Long Emission Wavelengths and Mega Stokes Shifts in 6-Aminocoumarins. *J. Phys. Chem. C* **2017,** *121* (24), 13274-13279.

35. Wu, X.; Tan, D.; Qiao, Q.; Yin, W.; Xu, Z.; Liu, X., Molecular Origins of the Multi-Donor Strategy in Inducing Bathochromic Shifts and Enlarging Stokes Shifts of Fluorescent Proteins. *Phys. Chem. Chem. Phys.* **2022,** *24* (26), 15937-15944.

36. Grabowski, Z. R.; Rotkiewicz, K.; Rettig, W., Structural Changes Accompanying Intramolecular Electron Transfer: Focuson Twisted Intramolecular Charge-Transfer States and Structures. *Chem. Rev.* **2003,** *103*.

37. Wang, C.; Chi, W.; Qiao, Q.; Tan, D.; Xu, Z.; Liu, X., Twisted Intramolecular Charge Transfer (TICT) and Twists Beyond TICT: From Mechanisms to Rational Designs of Bright and Sensitive Fluorophores. *Chem. Soc. Rev.* **2021,** *50* (22), 12656-12678.

38. Gao, Y.; Wang, C.; Chi, W.; Liu, X., Molecular Origins of Heteroatom Engineering on the Emission Wavelength Tuning, Quantum Yield Variations and Fluorogenicity of NBD-like SCOTfluors. *Chem. Asian J.* **2020,** *15* (23), 4082-4086.

39. Grimm, J. B.; English, B. P.; Chen, J.; Slaughter, J. P.; Zhang, Z.; Revyakin, A.; Patel, R.; Macklin, J. J.; Normanno, D.; Singer, R. H.; Lionnet, T.; Lavis, L. D., A General Method to Improve Fluorophores for Live-Cell and Single-Molecule Microscopy. *Nat. Methods* **2015,** *12* (3), 244-250.

40. Wang, C.; Qiao, Q.; Chi, W.; Chen, J.; Liu, W.; Tan, D.; McKechnie, S.; Lyu, D.; Jiang, X.-F.; Zhou, W.; Xu, N.; Zhang, Q.; Xu, Z.; Liu, X., Quantitative Design of Bright Fluorophores and AIEgens via the Accurate Prediction of Twisted Intramolecular Charge Transfer (TICT). *Angew. Chem. Int. Ed.* **2020,** *59*, 10160–10172.

41. Ding, N.; Liao, Y.-C.; Wang, G.; Chang, K.-H.; Wang, Z.; Liu, K.; Ma, J.; Chou, P.-T.; Fang, Y., Bi-*ortho*-Carborane Unit-Riveted Perylene Monoimides: Structure-Tuned Optical Switches for Electron Transfer and Robust Thin Film-Based Fluorescence Sensors. *CCS Chem.* **2023,** *5* (12), 2922-2932.